FRIEDRICH-SCHILLER-UNIVERSITÄT JENA

erc
European Research Council
Established by the European Commission

www.computational-relativity.org

Public database of NR BNS waveforms
https://core-gitlfs.tpi.uni-jena.de/core_database
and ejecta profiles
https://zenodo.org/communities/nrgw-opendata

Numerical relativity simulations and Gravitational wave modeling

S.Bernuzzi

INT 20R-1b
“The r-process and the nuclear EOS after LIGO-Virgo's third observing run”

May 2022

Outline

- Inspiral-merger GWs and measurement of tidal parameters (EOS)
  - Waveform models & systematics
  - Targets for future Numerical Relativity (NR) simulations
- Kilohertz GWs from merger remnants
  - Complete spectrum model (NR postmerger completion to inspiral-merger)
  - Detection of postmerger signals & additional EOS information (?)
- Prompt collapse
  - Equal vs unequal mass binaries
  - Maximum mass and nuclear incompressibility

Measuring tides: main challenge

PHYSICAL REVIEW D **85,** 123007 (2012)

Measurability of the tidal polarizability of neutron stars in late-inspiral gravitational-wave signals

Thibault Damour and Alessandro Nagar
Institut des Hautes Etudes Scientifiques, 91440 Bures-sur-Yvette, France ICRANet, 65122 Pescara, Italy

Loïc Villain
Laboratoire de Mathématiques et de Physique Théorique, Univ. F. Rabelais—CNRS (UMR 7350), Féd. Denis Poisson, 37200 Tours, France
(Received 20 March 2012; published 15 June 2012)

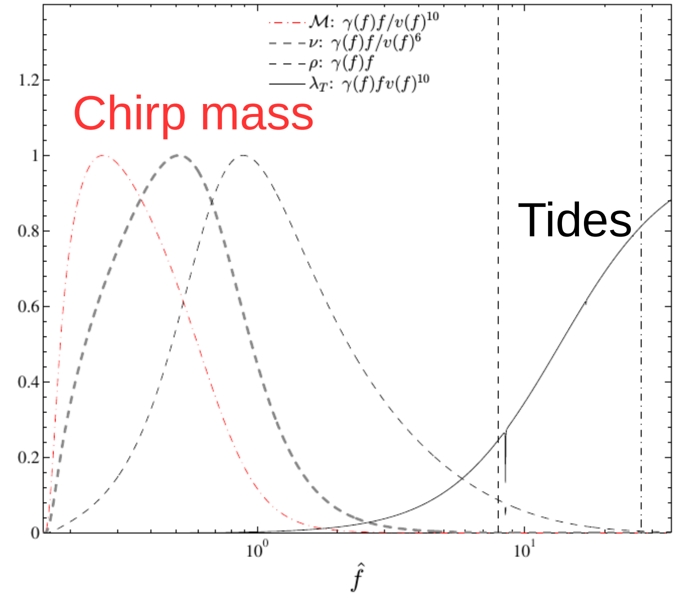

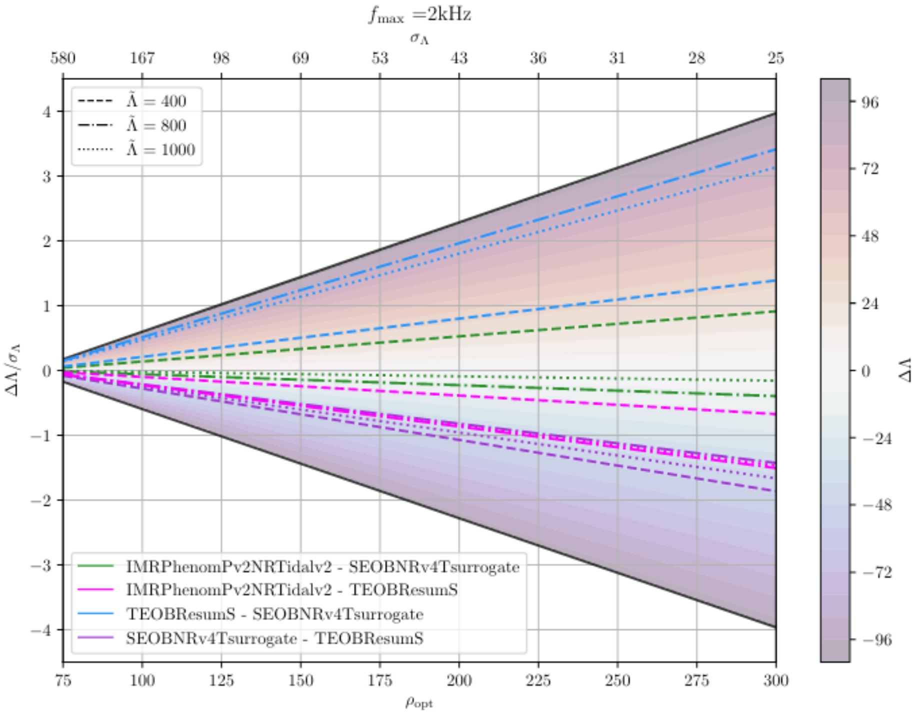

Gamba,Breschi,SB+ [https://arxiv.org/abs/2009.08467]

Tidal parameters inference & wvf systematics

Gamba, Breschi, SB+ [https://arxiv.org/abs/2009.08467]

Breschi+ [https://arxiv.org/abs/2101.01201]

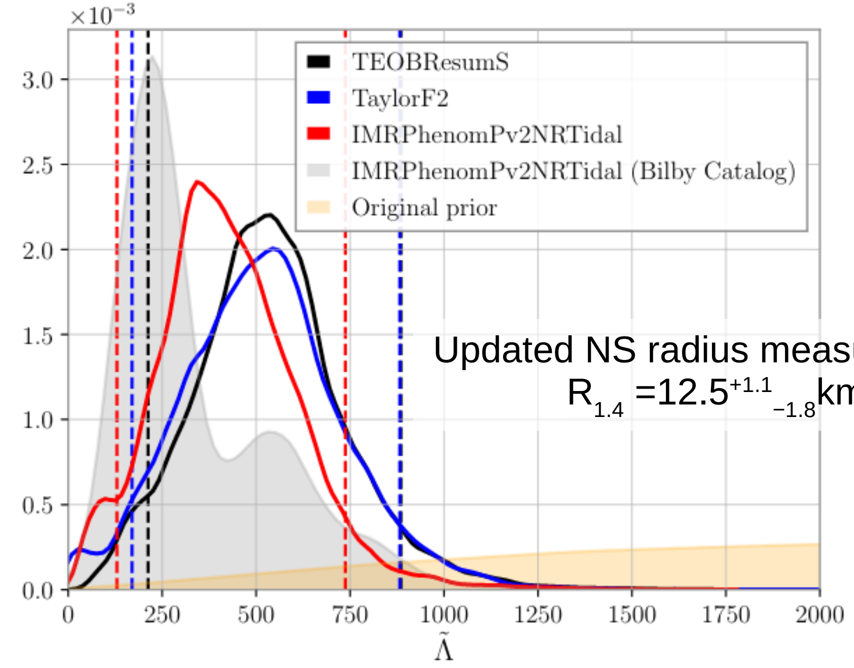

Updated NS radius measurement:
$R_{1.4} = 12.5^{+1.1}_{-1.8}$ km

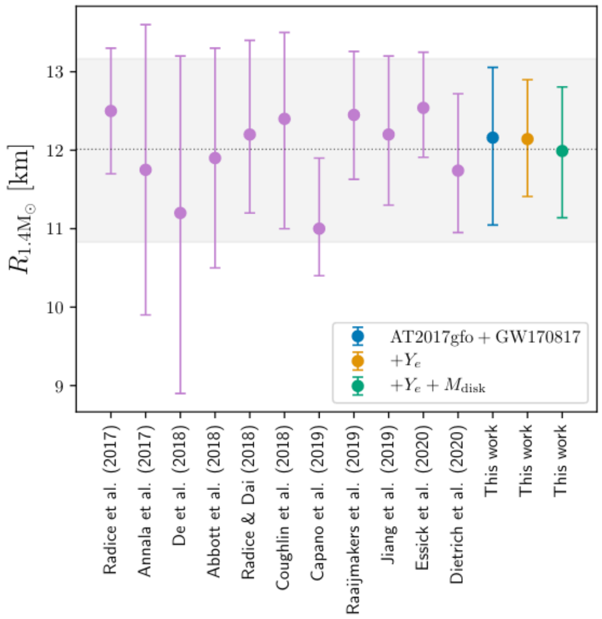

GW170817: no significant wvf systematics BUT $\tilde{\Lambda}$ “double peaked” posteriors …
1kHz cut-off removes double peaks, less wvf baises and shifts to larger $\tilde{\Lambda}$ (larger radii) for comparable log-like.
Estimated <10% SNR above f > 1kHz. High-frequencies issues in $\tilde{\Lambda}$-inference? [Dai+ 2018, Narikawa+ 2019]

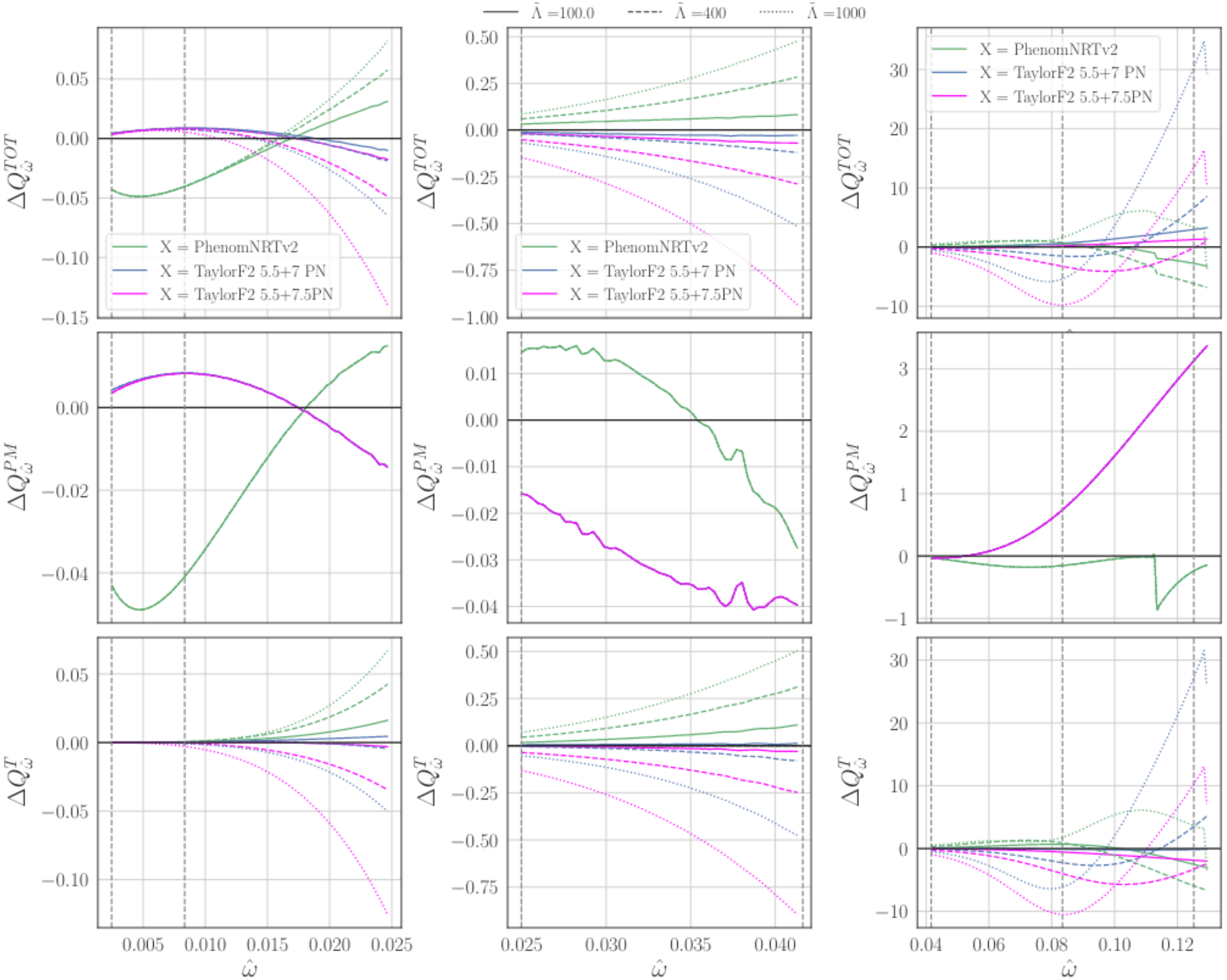

Total phasing

“point mass” phasing

Tidal phasing

Effective-one-body framework in a nutshell

[Buonanno&Damour PRD 2000a, 2000b]

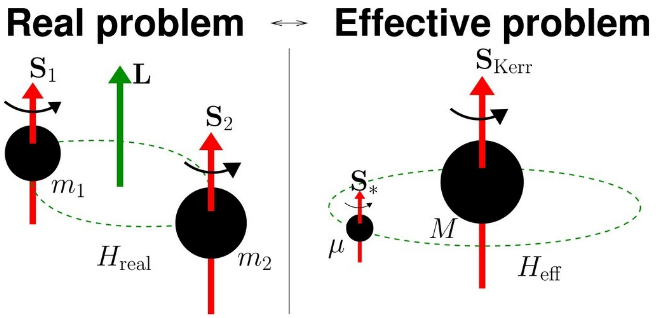

Credit: A.Taracchini

$$H_{\rm eff} \sim \mu\sqrt{A(u)(1+p_\phi^2 u^2)+p_{r^*}^2}$$

$$A(u;\nu;\kappa_2^T) = A^0(u;\nu) + A^T(u;\nu;\kappa_2^T)$$

$$A^0(u;\nu) = 1 - 2u + \nu(\dots$$

Factorized (resummed) PN waveform [Damour,Iyer,Nagar 2008]
Includes test-mass limit (i.e. particle on Schwarzschild)
Includes post-Newtonian and self-force results
Uses resummation techniques → predictive strong-field regime
Includes tidal interactions (→ BNS) [Damour&Nagar PRD 2010]
Flexible framework → NR informed

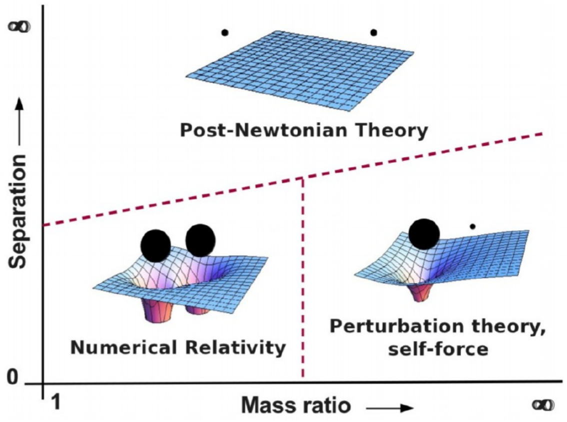

Credit: L.Barak

PHYSICAL REVIEW D **81,** 084016 (2010)

Effective one body description of tidal effects in inspiralling compact binaries

Thibault Damour and Alessandro Nagar
Institut des Hautes Etudes Scientifiques, 91440 Bures-sur-Yvette, France and ICRANet, 65122 Pescara, Italy
(Received 26 November 2009; published 8 April 2010)

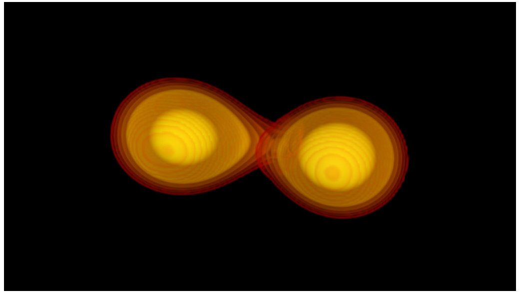

$$\kappa_2^T = 2\left[\frac{X_A}{X_B}\left(\frac{X_A}{C_A}\right)^5 k_2^A + \frac{X_B}{X_A}\left(\frac{X_B}{C_B}\right)^5 k_2^B\right]$$

Tidal coupling constant (Analogous to the reduced tidal parameter $\bar{\Lambda}$ [Favata 2013])

Hamiltonian
(Newtonian limit):

$$H_{\mathrm{EOB}} \approx Mc^2 + \frac{\mu}{2}\left(\mathbf{p}^2 + A(r) - 1\right)$$

$$A(r) = 1 - \frac{2}{r} - \frac{\kappa_2^T(k_2)}{r^6}$$

Waveform:

$$h \sim Af^{-7/6}e^{-i\Psi(x(f))} = Af^{-7/6}e^{-i\Psi_{\mathrm{pp}}(x)+i39/4\,\kappa_2^T x^{5/2}}$$

A PN @ NNLO insufficient to merger ! (SB+ [https://arxiv.org/abs/1205.3403])

PRL **114,** 161103 (2015) PHYSICAL REVIEW LETTERS week ending 24 APRIL 2015

Modeling the Dynamics of Tidally Interacting Binary Neutron Stars up to the Merger

Sebastiano Bernuzzi,[1,2] Alessandro Nagar,[3] Tim Dietrich,[4] and Thibault Damour[3]
[1]TAPIR, California Institute of Technology, Pasadena, California 91125-0001, USA
[2]DiFeST, University of Parma, I-43124 Parma, Italy
[3]Institut des Hautes Etudes Scientifiques, 91440 Bures-sur-Yvette, France
[4]Theoretical Physics Institute, University of Jena, 07743 Jena, Germany
(Received 15 December 2014; revised manuscript received 18 February 2015; published 23 April 2015)

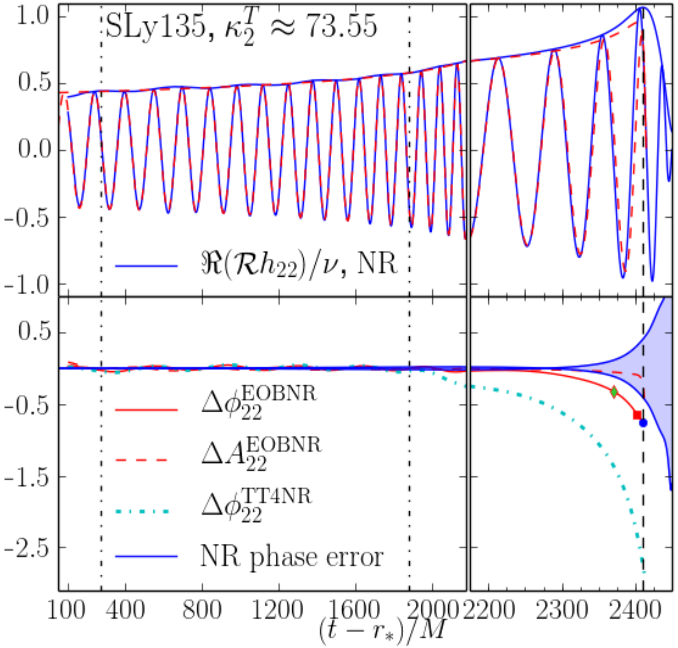

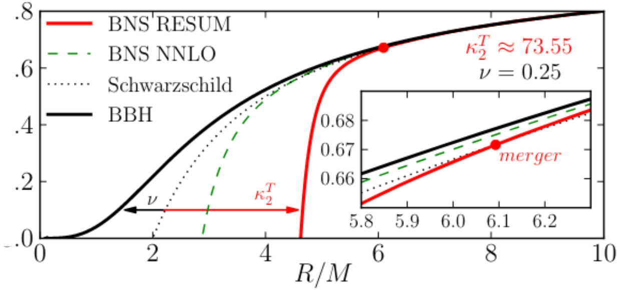

FIG. 1: The main radial gravitational potential $A(R)$ in various EOB models. Finite-mass ratio effects (ν) make the gravitational interaction less attractive than the Schwarzschild relativistic potential $A_{\rm Schw} = 1 - 2M/R$, while tides (κ_2^T, see Table I) make it more attractive (especially at short separations).

PHYSICAL REVIEW D **90,** 124037 (2014)

Gravitational self-force corrections to two-body tidal interactions and the effective one-body formalism

Donato Bini[1] and Thibault Damour[2]
[1]Istituto per le Applicazioni del Calcolo "M. Picone," CNR, I-00185 Rome, Italy
[2]Institut des Hautes Etudes Scientifiques, 91440 Bures-sur-Yvette, France
(Received 24 September 2014; published 10 December 2014)

See also Bini, Damour, Feye 2013, Dolan+ 2014
Akcay, SB+ [https://arxiv.org/abs/1812.02744]

Dynamical Tides in General Relativity: Effective Action and Effective-One-Body Hamiltonian

Jan Steinhoff,[1,2] Tanja Hinderer,[3,1] Alessandra Buonanno,[1,3] and Andrea Taracchini[1]
[1]*Max Planck Institute for Gravitational Physics (Albert Einstein Institute), Am Mühlenberg 1, Potsdam 14476, Germany*
[2]*Centro Multidisciplinar de Astrofísica — CENTRA, Departamento de Física, Instituto Superior Técnico — IST, Universidade de Lisboa — ULisboa, Avenida Rovisco Pais 1, 1049-001 Lisboa, Portugal*
[3]*Department of Physics, University of Maryland, College Park, MD 20742, USA*
(Dated: November 17, 2016)

See also e.g.
Lai [https://arxiv.org/abs/astro-ph/9404062]
Kokkotas&Schaefer [https://arxiv.org/abs/gr-qc/9502034]

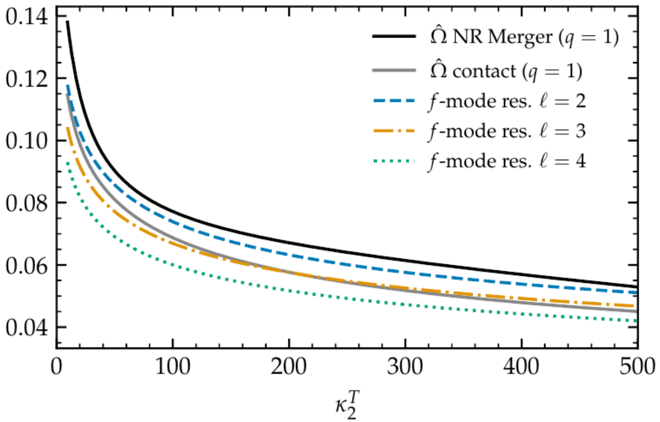

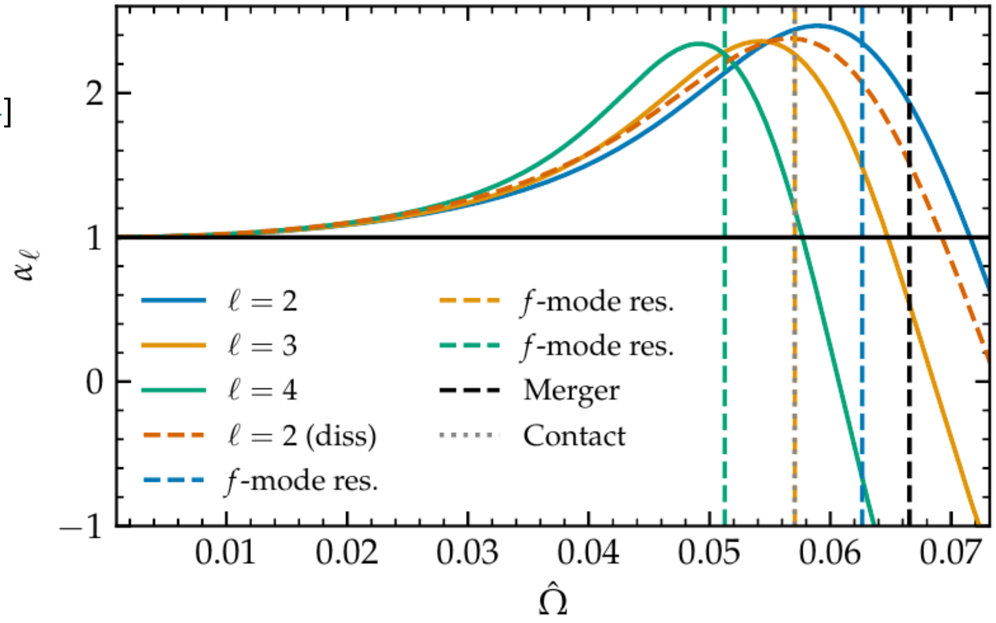

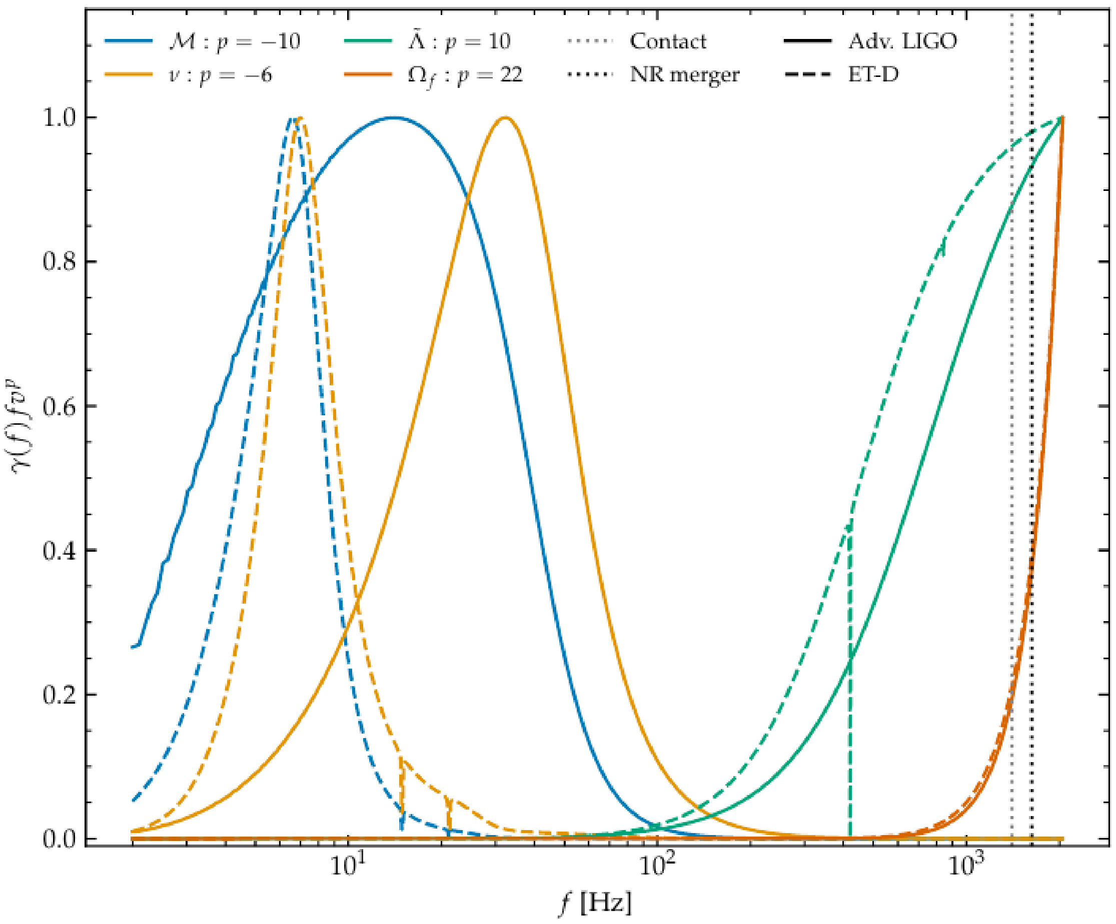

Preliminary
Gamba,SB

Closed-form tidal approximants for binary neutron star gravitational waveforms constructed from high-resolution numerical relativity simulations

Tim Dietrich[1], Sebastiano Bernuzzi[2,3], and Wolfgang Tichy[4]

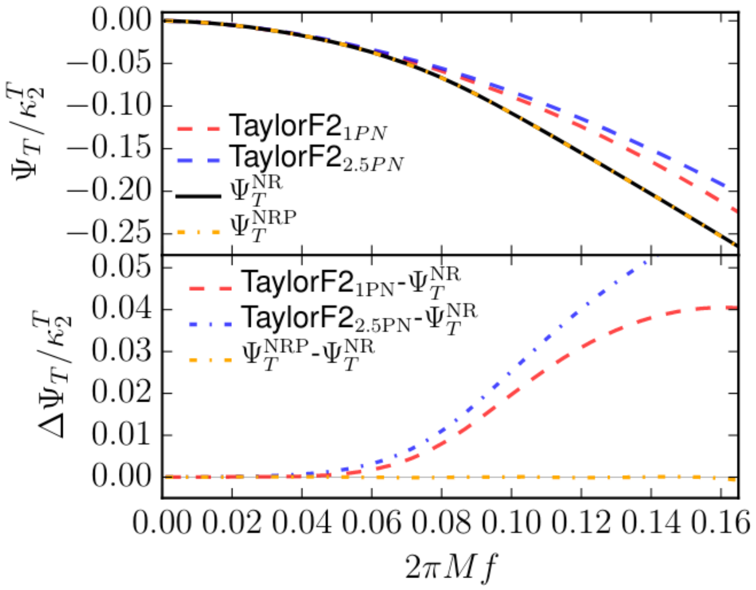

FIG. 3. Frequency-domain tidal approximants. Top panel shows $\Psi_T/\kappa^T_{\rm eff}$ as given by the TaylorF2$_{\rm 1PN}$, TaylorF2$_{\rm 2.5PN}$ [32], Eq. (6), and Eq. (7). Bottom panel: Difference between the frequency-domain representations.

$$\phi(\hat\omega) \approx \phi_0(\hat\omega) + \phi_{SO}(\hat\omega) + \phi_T(\hat\omega)$$

$$\frac{d^2\Psi_T^{\rm SPA}}{d\omega_f^2} = \frac{Q_\omega(\omega_f)}{\omega_f^2}$$

$$\Psi_T^{\rm NRP} = -\kappa^T_{\rm eff}\frac{\tilde c_{\rm Newt}}{X_A X_B} x^{5/2} \times \frac{1+\tilde n_1 x + \tilde n_{3/2} x^{3/2} + \tilde n_2 x^2 + \tilde n_{5/2} x^{5/2}}{1+\tilde d_1 x + \tilde d_{3/2} x^{3/2}}$$

Accuracy of NR waveforms

TABLE V. Faithfulness values $\mathcal{F}$ computed considering frequencies from $f_{\rm low}$ to $f_{\rm mrg}$ between simulations with the same intrinsic parameters and two different resolutions, extracted at $r/M = 1000$. The source is situated in the same sky location as GW170817, and the waveform polarizations h_+ and $h_\times$ are computed and projected on the Livingston detector. We employ the `aLIGODesignSensitivityP1200087` [22] PSD from `pycbc` [110] to compute the matches, and compare the values obtained to the thresholds $\mathcal{F}_{\rm thr}$ calculated with Eq. 19 with $\epsilon^2 = 1$ or $\epsilon^2 = N$. A tick ✓ indicates that $\mathcal{F} > \mathcal{F}_{\rm thr}$. Conversely, a cross ✗ indicates that $\mathcal{F} < \mathcal{F}_{\rm thr}$.

Sim	n[a]	$\mathcal{F}$	SNR 14		30		80	
			$N=6$	1	$N=6$	1	$N=6$	1
BAM:0011	[96, 64]	0.991298	✓	✗	✗	✗	✗	✗
BAM:0017	[96, 64]	0.985917	✓	✗	✗	✗	✗	✗
BAM:0021	[96, 64]	0.957098	✗	✗	✗	✗	✗	✗
BAM:0037	[216, 144]	0.998790	✓	✓	✓	✗	✗	✗
BAM:0048	[108, 72]	0.983724	✗	✗	✗	✗	✗	✗
BAM:0058	[64, 64]	0.999127	✓	✓	✓	✗	✗	✗
BAM:0064	[240, 160]	0.997427	✓	✗	✓	✗	✗	✗
BAM:0091	[144, 108]	0.997810	✓	✓	✓	✗	✗	✗
BAM:0094	[144, 108]	0.996804	✓	✗	✓	✗	✗	✗
BAM:0095	[256, 192]	0.999550	✓	✓	✓	✓	✓	✗
BAM:0107	[128, 96]	0.995219	✓	✗	✗	✗	✗	✗
BAM:0127	[128, 96]	0.999011	✓	✓	✓	✗	✗	✗

[a] Number of grid point (linear resolution) of the finest grid refinement, roughly covering the diameter of one NS

Gamba,Breschi,SB+[https://arxiv.org/abs/2009.08467]

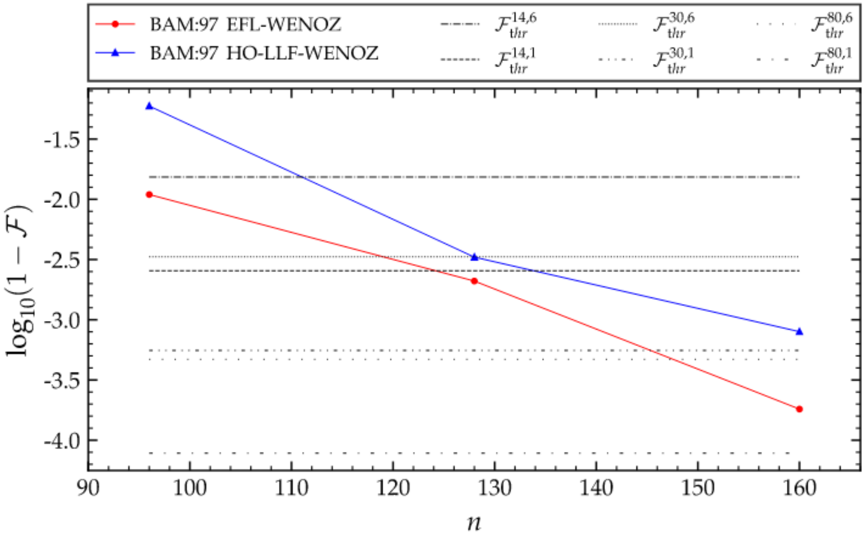

FIG. 21. Faithfulness as a function of the resolution for the BAM:97 simulation.

Doulis,Atteneder,SB,Bruegmann [https://arxiv.org/abs/2202.08839]

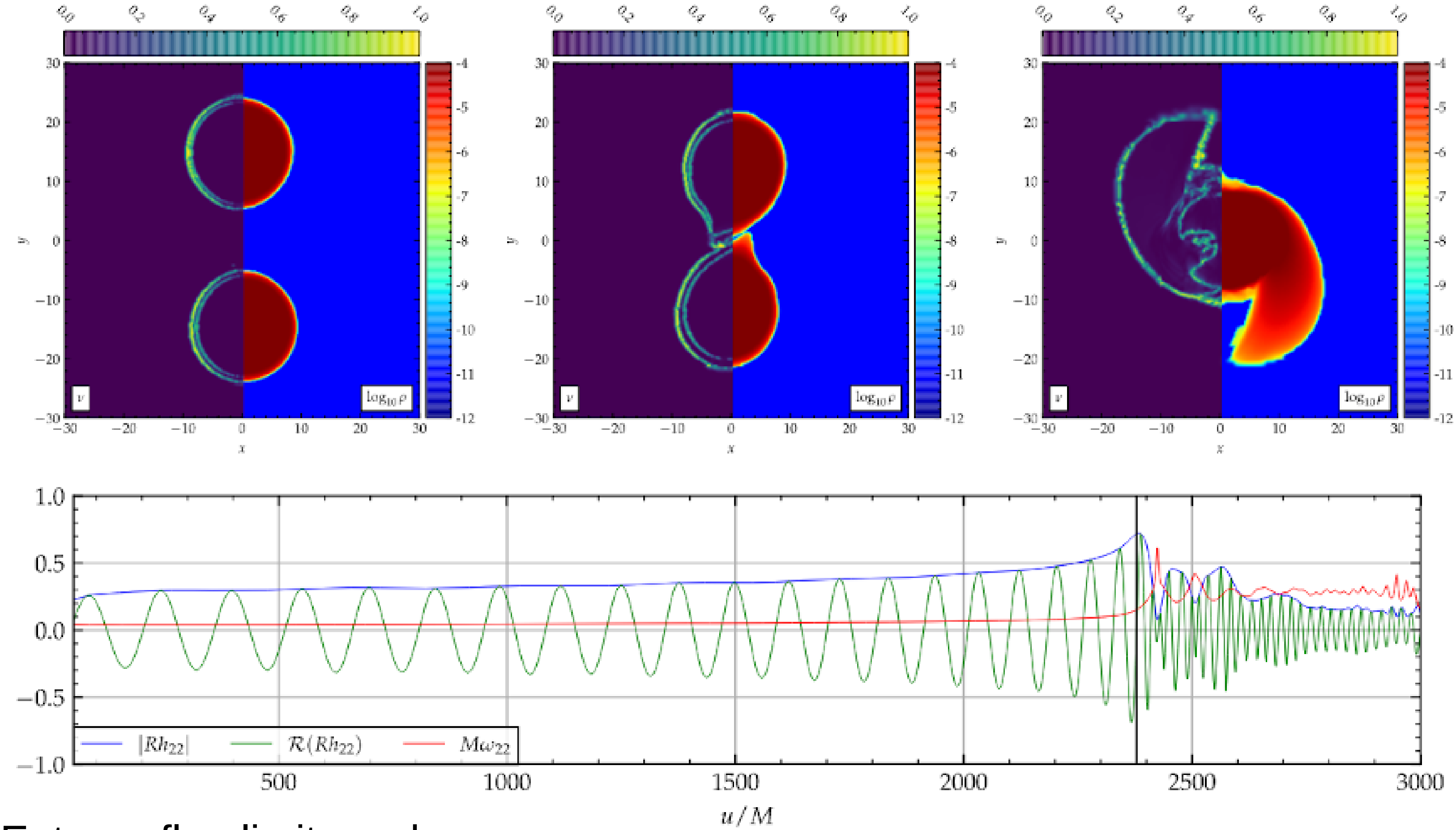

Entropy flux-limiter scheme

Doulis,Atteneder,SB,Bruegmann [https://arxiv.org/abs/2202.08839]

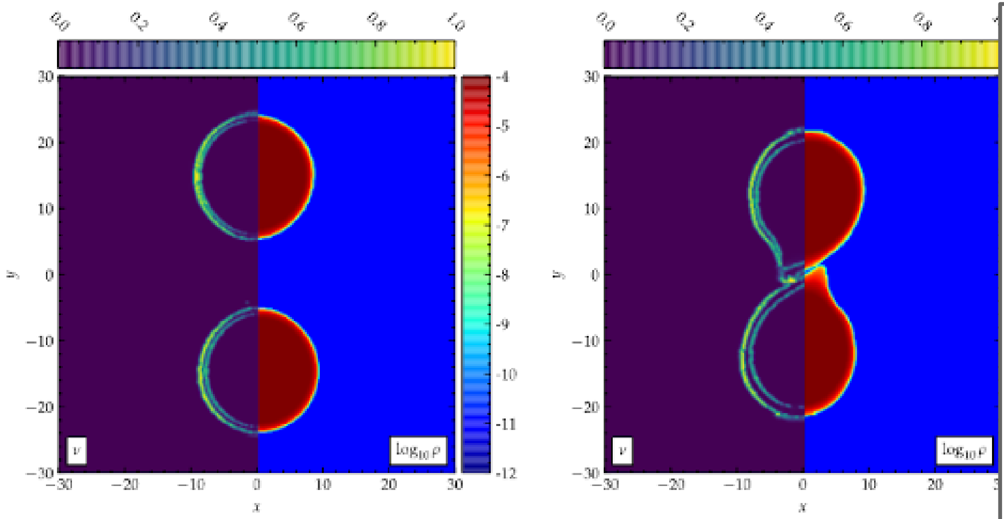

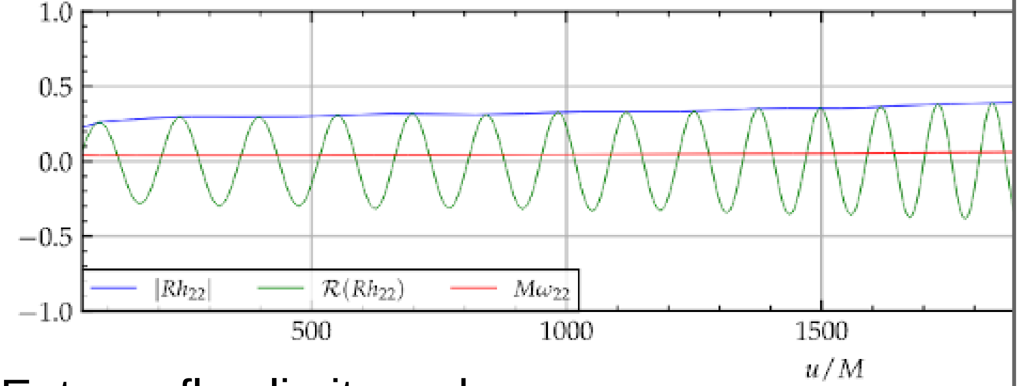

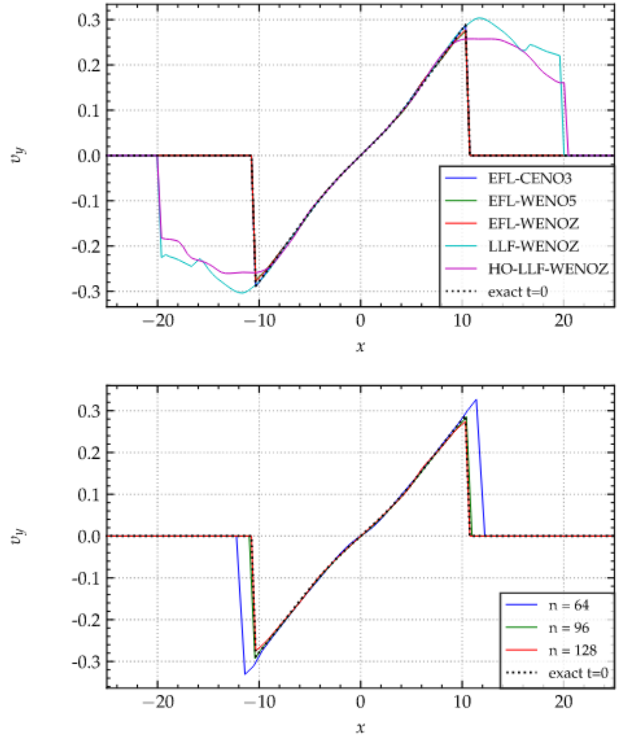

FIG. 9. Velocity profile of a stationary rotating neutron star in a dynamical spacetime with Γ-law EoS. Top: One-dimensional profile of the velocity component v_y along the x-direction at time $t = 1000$ (four periods) with $n = 128$. Bottom: The v_y profile of the WENO5 scheme with increasing resolution.

Entropy flux-limiter scheme

Doulis,Atteneder,SB,Bruegmann [https://arxiv.org/abs/2202.08839]

High-order schemes, eccentricity-controlled initial data and code comparisons

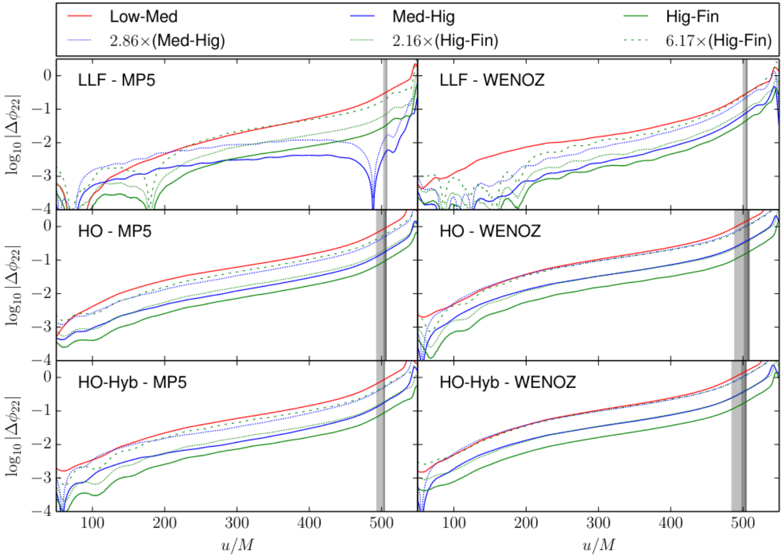

FIG. 9. Convergence of SLy135135_006. The different panels show the phase differences in log scale for different reconstructions: MP5 (left) and WENOZ (right). The algorithms from top to bottom are: LLF, HO, HO-Hyb. The vertical shaded regions represent the moment of merger for different resolutions: light gray for $[u^{L}_{mrg}, u^{M}_{mrg}]$, gray for $[u^{M}_{mrg}, u^{H}_{mrg}]$ and dark gray for $[u^{H}_{mrg}, u^{F}_{mrg}]$. To show convergence we rescale the phase differences assuming second-order convergence, cf. dashed and dot-dashed lines.

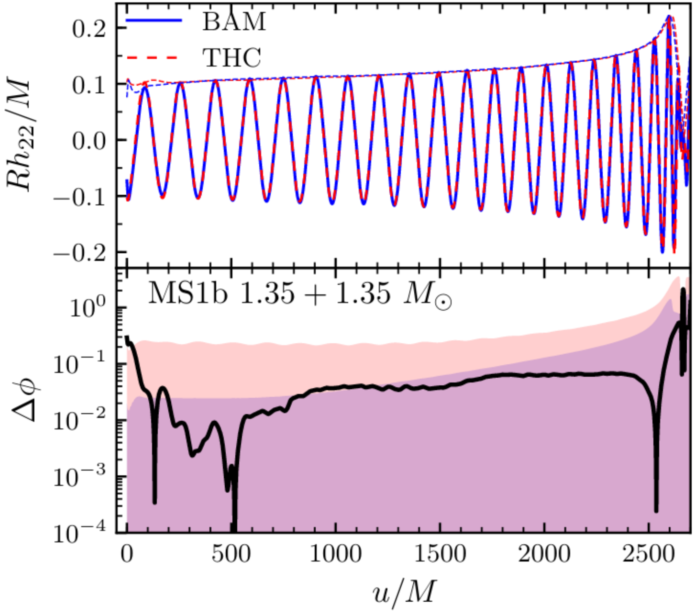

FIG. 31. Systematic uncertainties in BNS numerical relativity inspiral-merger waveform. Waveforms from two independent and high-order codes are compared.

SB&Dietrich [https://arxiv.org/abs/1604.07999]
See also Radice+ [https://arxiv.org/abs/1306.6052]

Initial data:
Moldenhauer+ [https://arxiv.org/abs/1408.4136]
Tichy [https://arxiv.org/abs/1209.5336]

Nagar,SB,…,Radice+ [https://arxiv.org/abs/1806.01772]

The BNS gravitational-wave spectrum

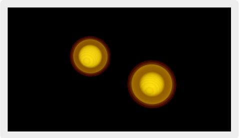

SB+ [https://arxiv.org/abs/1504.01764]
Breschi,SB+ [https://arxiv.org/abs/1908.11418]
Breschi,SB+ [https://arxiv.org/abs/2205.09112]

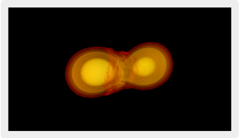

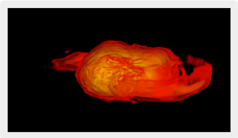

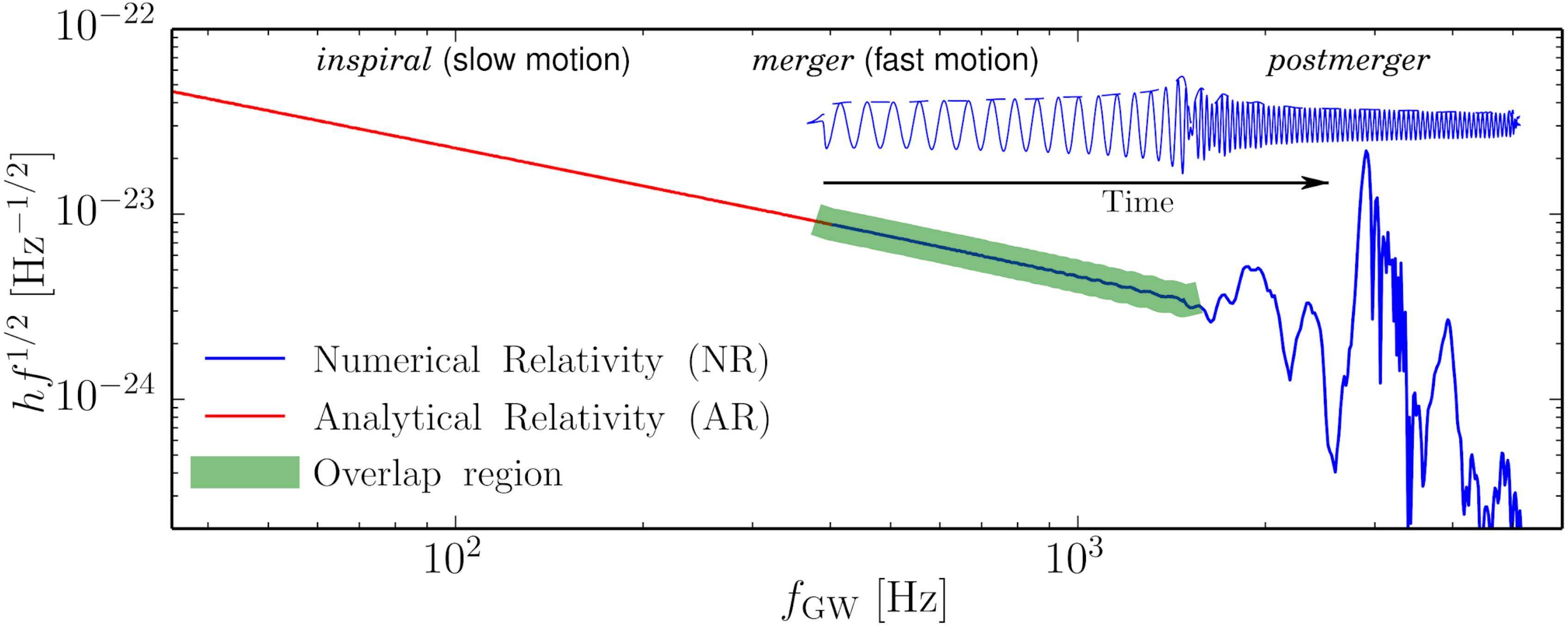

Breschi,SB+ [https://arxiv.org/abs/2205.09112]

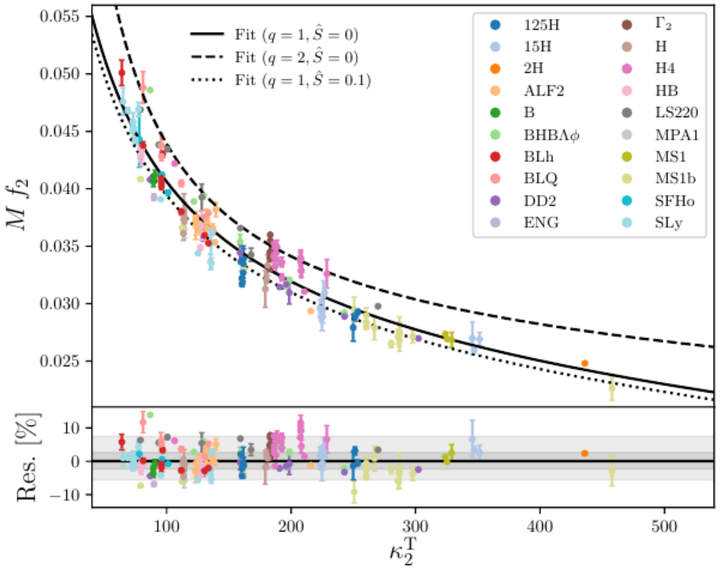

FIG. 3. Quasi-universal relation for the PM peak frequency f_2 as function of the tidal polarizability κ_2^T. Top panel: calibrated relations (black lines) compared to NR data (colored dots) extracted from the CoRe and the SACRA databases. Each color corresponds to a different EOS. NR medians and error-bars are reported averaging over different numerical resolutions (when available) for the same binary configuration. Bottom panel: Relative residuals between the calibrated relation and the NR data validation set. The gray areas show the 50% (dark) and 90% (light) credible regions of the residuals.

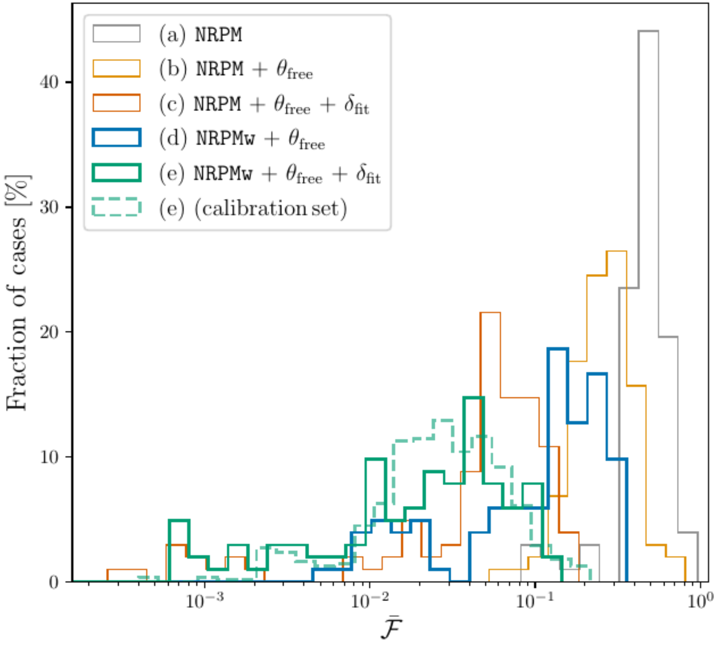

FIG. 5. Recovered unfaithfulness $\bar{\mathcal{F}}$ between PM models and NR data of the validation set [11, 56, 61, 72, 88, 110] employing ET-D sensitivity [2, 3]. For NRPM [11] (thin lines), we compute $\bar{\mathcal{F}}$ with the standard model (a), including PM parameters (b) and also the recalibrations (c). Analogously, the $\bar{\mathcal{F}}$ recovered for NRPMw (thick lines) include the PM parameters (d) and also the recalibrations (e). The dashed histogram shows the $\bar{\mathcal{F}}$ for case (e) computed over the calibration set.

Post-merger detection with 3G

Breschi,SB+ [https://arxiv.org/abs/2205.09112]

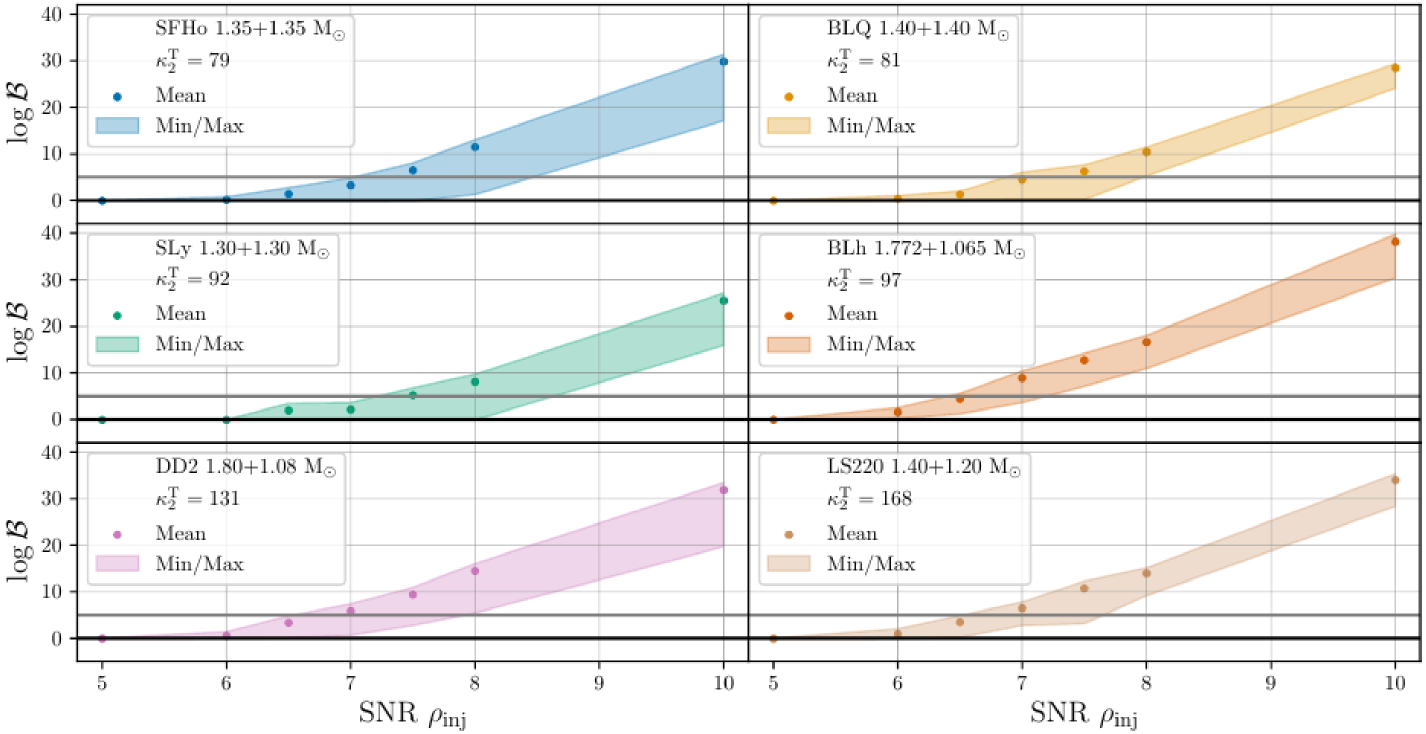

FIG. 5. Logarithmic BFs $\log \mathcal{B}$ as functions of the PM SNR $\rho_{\rm inj}$ of the injected NR template from Table I. The dots refer to the mean values averaged over the different noise realizations and the shadowed areas correspond to the minimum and maximum values recovered in the survey. Two horizontal lines identify $\log \mathcal{B} = 0$ (black) and $\log \mathcal{B} = 5$ (gray).

Full-spectrum constraints on M-R diagram

Full-spectrum (mock) analysis using ET @ minimum SNR threshold for a PM detection
NS maximum density to 15% and maximum mass to 12% (90% conf. Lev.)
Recalibration parameters: account for theoretical uncertainties in EOS-insensitive rel.

Breschi, SB+ [https://arxiv.org/abs/2110.06957]

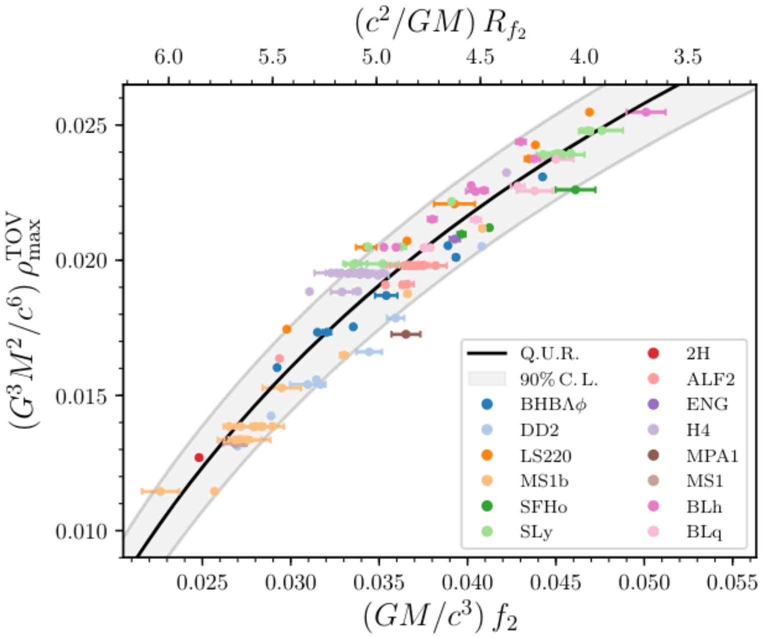

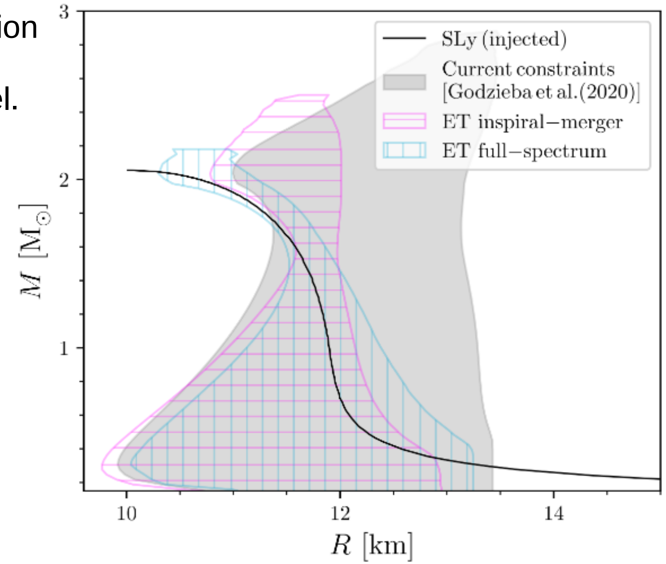

FIG. 4. Mass-radius diagram constraints from a single full-spectrum Einstein Telescope (ET) BNS observation with PM SNR 10 (total SNR 180). The gray area (prior) corresponds to the two-million EOS sample of Ref. [69]. The magenta and cyan areas are the 90% credibility regions given by inspiral-merger and inspiral-merger-PM inferences respectively. The full-spectrum (cyan) posterior agrees with the injected EOS (black).

Deviations from quasiuniversal relations

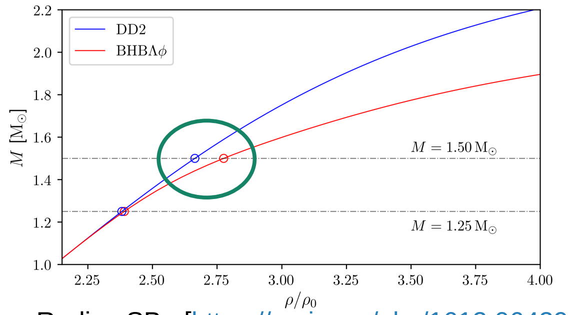

Radice,SB+ [https://arxiv.org/abs/1612.06429]

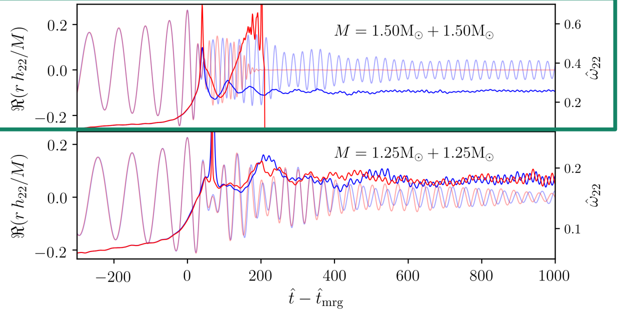

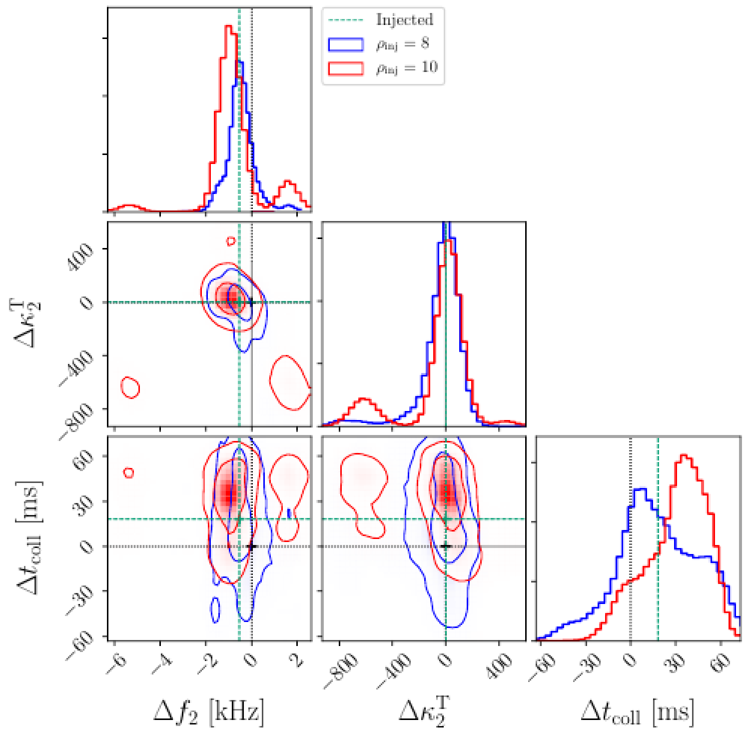

Small “window” of binary parameters (EOS dependent)
Frequency vs collapse time
Recalibration parameters: are critical here 1,2,...N-sigma (?!)

Be careful concluding something about your favorite EOS model!

Breschi,SB+ [https://arxiv.org/abs/1908.11418]
Breschi+ [https://arxiv.org/abs/2205.09979]

Prompt collapse: equal masses

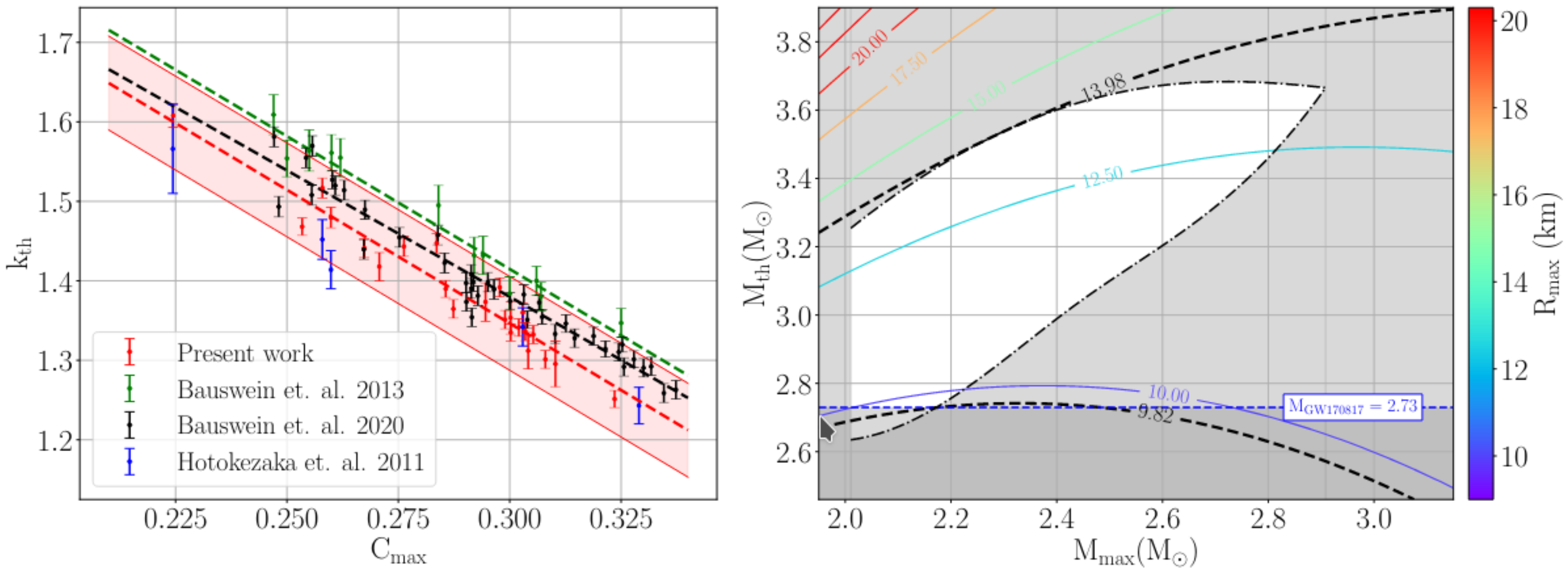

FIG. 4: *Left panel:* Plot of k_{th} vs. C_{max} from present and previous works [11, 18, 22]. Fits are constructed using our data and are shown in combination with the data of Hotokezaka *et al.* [11], Bauswein *et al.* [18] and Bauswein *et al.* [22]. The weighted linear regression results take into account the uncertainty in k_{th}. The shaded region represents uncertainties in the intercept. *Right panel:* Constraints on the R_{max}, M_{max} and M_{th} obtained using the correlation in left panel, PWP phenomenological constraints in combination with the observational lower limit on the maximum mass of nonrotating neutron stars and total mass of the event GW170817 as the lowest limit for prompt collapse.

Kashyap+ [https://arxiv.org/abs/2111.05183]

Inferring BH formation from inspiral GW

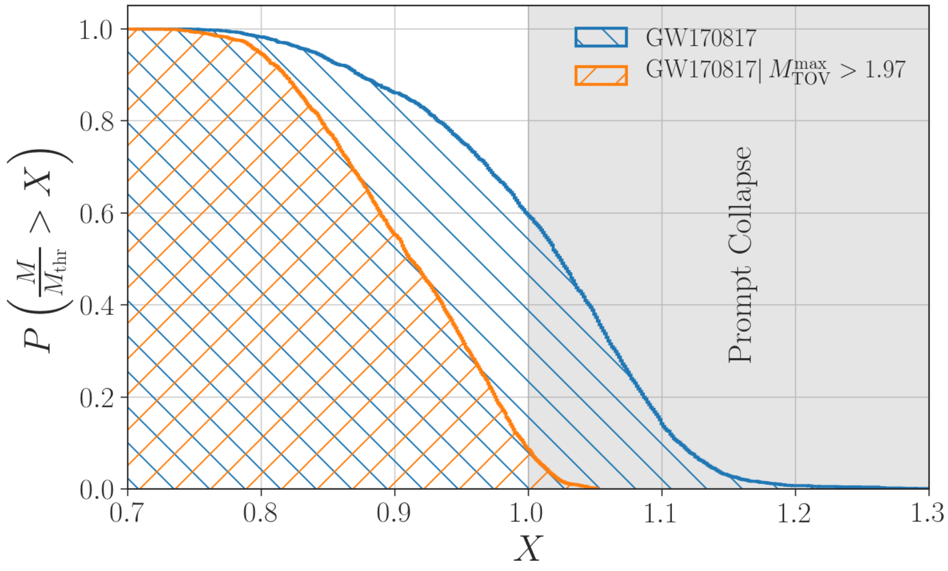

$P_{GW170817}$(prompt collapse|M<1.97) < 10%

- Two methods, w/ NR-based prompt collapse criteria (consistent results)
  - EOS inference + Threshold mass
  - Tidal parameter + Λ-Threshold
- GW170817: quantitatively support the "mainstream" interpretation of counterparts
- GW190425:

$P_{GW190425}$(prompt collapse) ~ 97%

LVC [https://arxiv.org/abs/2001.01761]

Agathos, Zappa, SB+ [https://arxiv.org/abs/1908.05442]

Prompt collapse: unequal masses

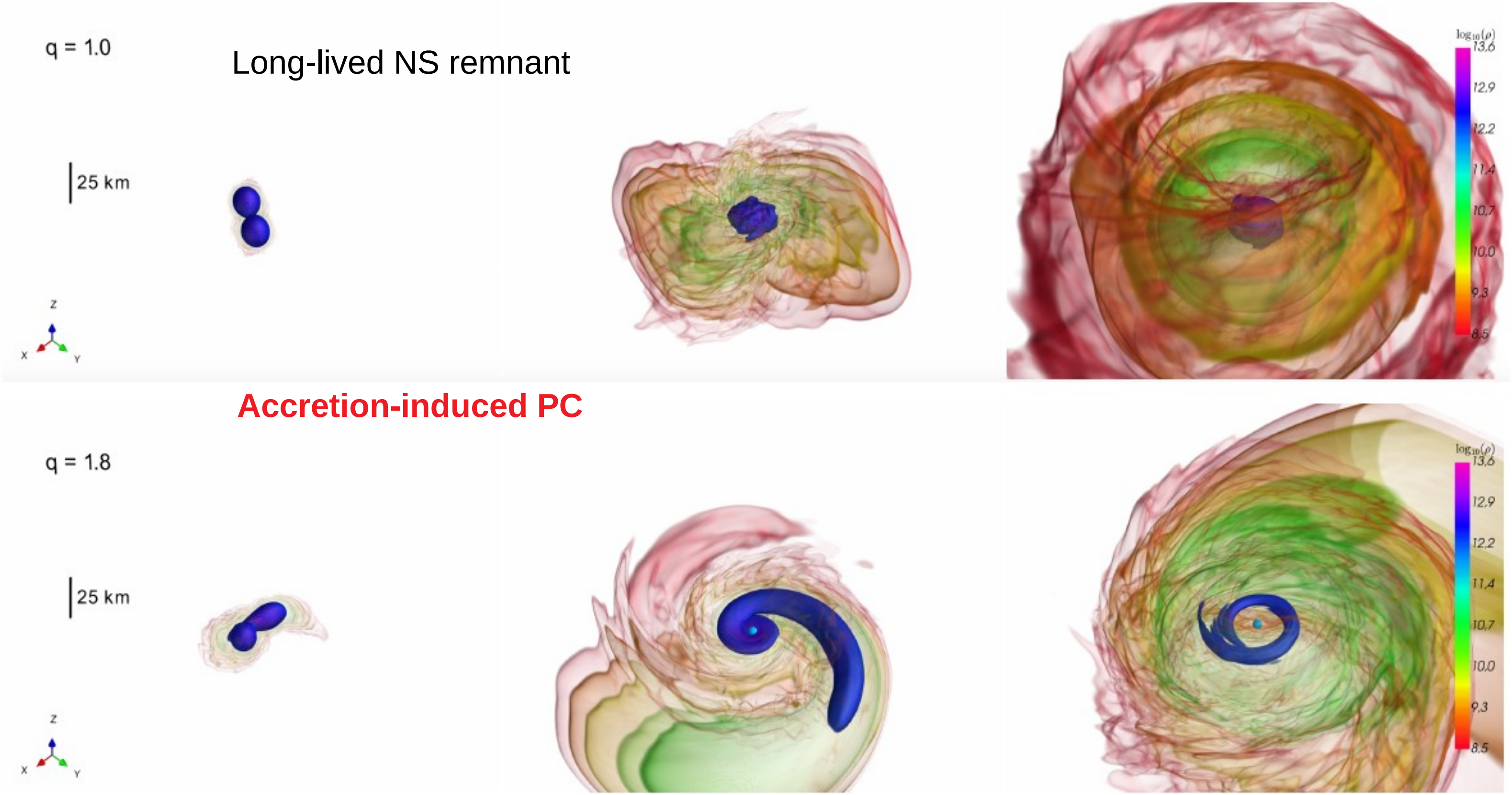

SB+ [https://arxiv.org/abs/2003.06015]

Prompt collapse: unequal masses

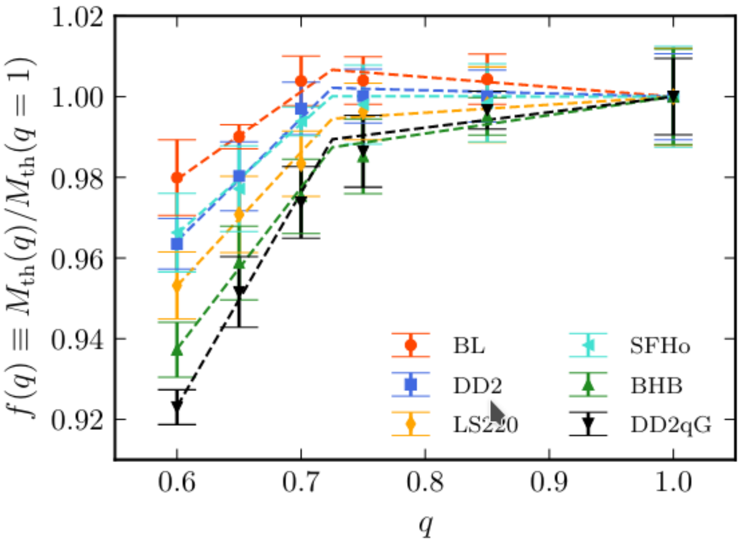

FIG. 2. Threshold PC masses normalized to the $q = 1$ case as a function of q for all the EOS used in this work. Dashed lines correspond to Eq. (2) fit.

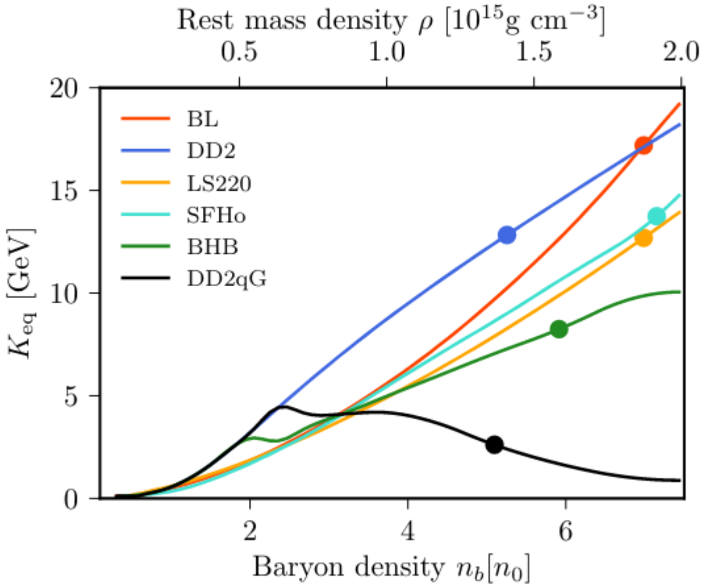

FIG. 1. Nuclear incompressibility $K_{\rm eq}$ of cold, β-equilibrated nuclear matter as a function of baryon density for the EOSs employed in this work. Solid markers correspond to $K_{\max}$, i.e. $K_{\rm eq}$ at the central density of the heaviest, irrotational NS.

Perego+ [https://arxiv.org/abs/2112.05864]

Disagreement NR+mesh vs conformally-flat+SPH simulations

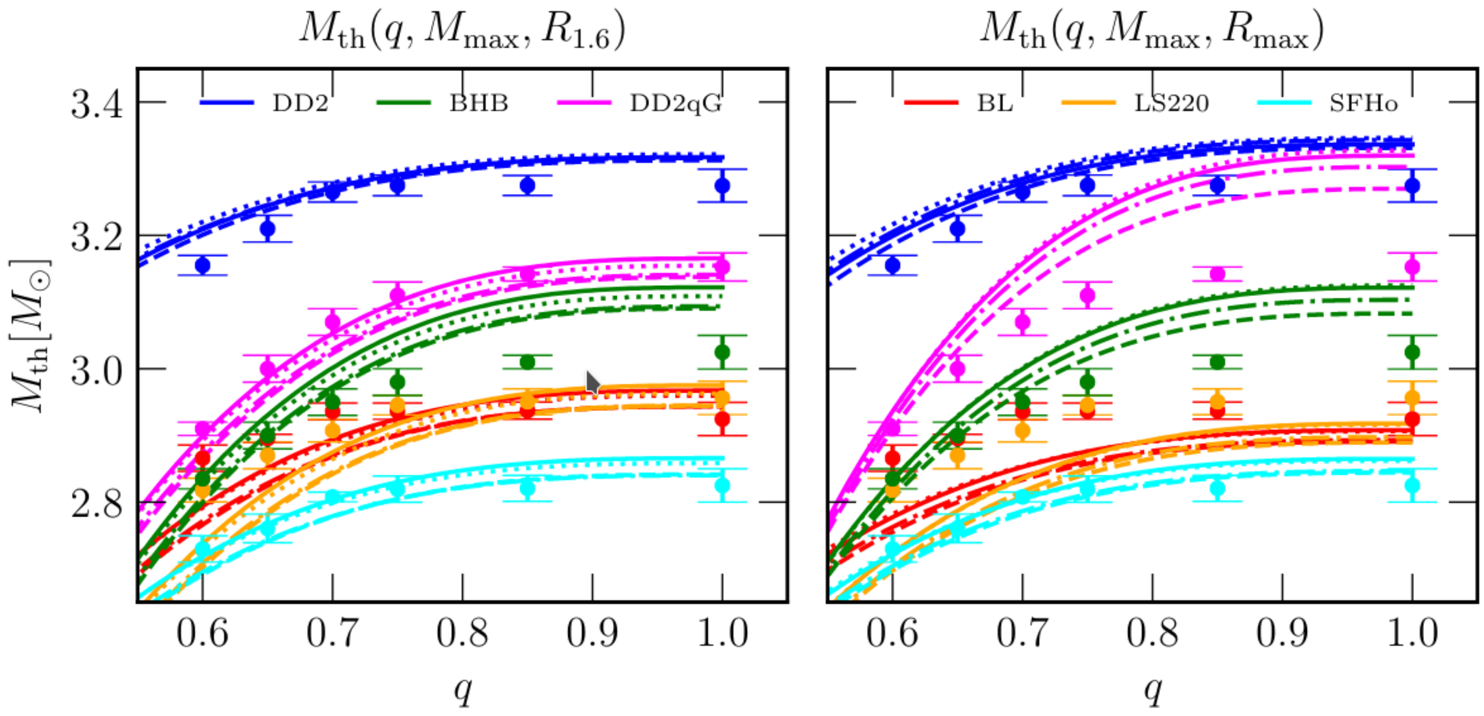

FIG. 8. Comparison between our results (dots) and the q-dependent fit results presented in [59], equation 10 and table VI. Different colors refer to the six EOS used in our work, while different lines correspond to different EOS samples employed in Table IV of [59]. In particular, we include the baseline "b" sample (solid), the "b+h" sample (dashed), the "b+e" sample (dotted) and the "b+h+e" sample (dash-dotted).

Summary & thanks!

- Inspiral-merger GWs and measurement of tidal parameters (EOS)
  - Current waveform models insufficient at SNR>80
  - NR simulations at higher precision necessary for last cycles

Gamba+ [https://arxiv.org/abs/2009.08467]

- Kilohertz GWs from merger remnants
  - NR-informed complete spectrum model
  - Detection of postmerger signals at postmerger SNR~7 (inspiral SNR>100!)
  - Extra EOS information tricky to extract

Breschi+ [https://arxiv.org/abs/2205.09112]

- Prompt collapse
  - Maximum mass from equal-mass binaries appear robust
  - Accretion-induced collapse rich phenonemology (nuclear incompressibility)

Perego+ [https://arxiv.org/abs/2112.05864]

Backup slides

Love numbers depends on EOS and NS compactness

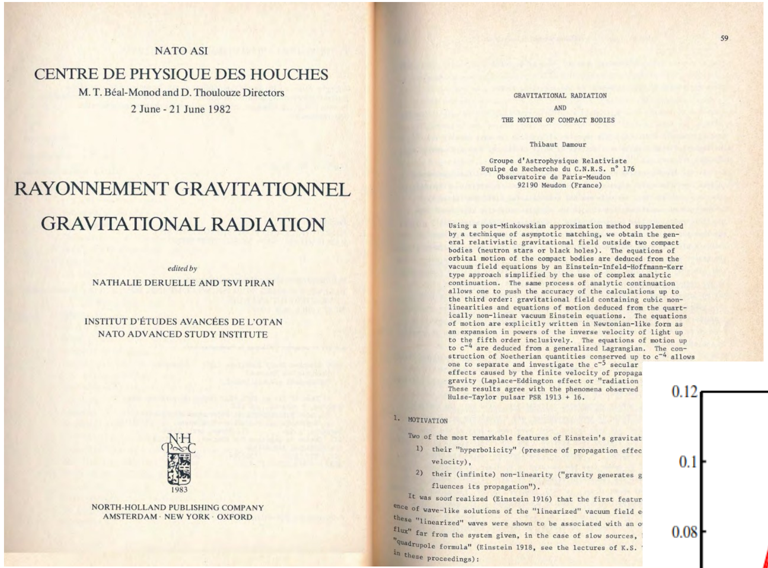

NATO ASI

CENTRE DE PHYSIQUE DES HOUCHES

M. T. Béal-Monod and D. Thoulouze Directors

2 June - 21 June 1982

RAYONNEMENT GRAVITATIONNEL

GRAVITATIONAL RADIATION

edited by

NATHALIE DERUELLE AND TSVI PIRAN

INSTITUT D'ÉTUDES AVANCÉES DE L'OTAN
NATO ADVANCED STUDY INSTITUTE

1983

NORTH-HOLLAND PUBLISHING COMPANY
AMSTERDAM · NEW YORK · OXFORD

59

GRAVITATIONAL RADIATION
AND
THE MOTION OF COMPACT BODIES

Thibault Damour

Groupe d'Astrophysique Relativiste
Equipe de Recherche du C.N.R.S. n° 176
Observatoire de Paris-Meudon
92190 Meudon (France)

Using a post-Minkowskian approximation method supplemented by a technique of asymptotic matching, we obtain the general relativistic gravitational field outside two compact bodies (neutron stars or black holes). The equations of orbital motion of the compact bodies are deduced from the vacuum field equations by an Einstein-Infeld-Hoffmann-Kerr type approach simplified by the use of complex analytic continuation. The same process of analytic continuation allows one to push the accuracy of the calculations up to the third order: gravitational field containing cubic nonlinearities and equations of motion deduced from the quartically non-linear vacuum Einstein equations. The equations of motion are explicitly written in Newtonian-like form as an expansion in powers of the inverse velocity of light up to the fifth order inclusively. The equations of motion up to c^{-4} are deduced from a generalized Lagrangian. The construction of Noetherian quantities conserved up to c^{-4} allows
one to separate and investigate the c^{-5} secular
effects caused by the finite velocity of propaga
gravity (Laplace-Eddington effect or "radiation
These results agree with the phenomena observed
Hulse-Taylor pulsar PSR 1913 + 16.

1. MOTIVATION

Two of the most remarkable features of Einstein's gravitat
1) their "hyperbolicity" (presence of propagation effec
velocity),
2) their (infinite) non-linearity ("gravity generates g
fluences its propagation").

It was soon realized (Einstein 1916) that the first featur
ence of wave-like solutions of the "linearized" vacuum field e
these "linearized" waves were shown to be associated with an o
flux" far from the system given, in the case of slow sources,
"quadrupole formula" (Einstein 1918, see the lectures of K.S.
in these proceedings):

"inner problem"

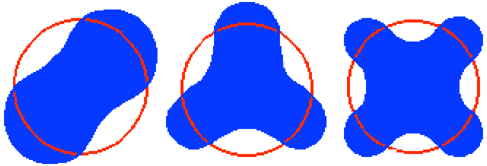

$$Q_{ij} = \lambda_2 G_{ij} \sim \lambda_2 \partial_i \partial_j \phi$$

PHYSICAL REVIEW D **80**, 084035 (2009)

Relativistic tidal properties of neutron stars

Thibault Damour[1,2] and Alessandro Nagar[1,2]
[1]*Institut des Hautes Etudes Scientifiques, 91440 Bures-sur-Yvette, France*
[2]*ICRANet, 65122 Pescara, Italy*

(Received 30 May 2009; published 23 October 2009)

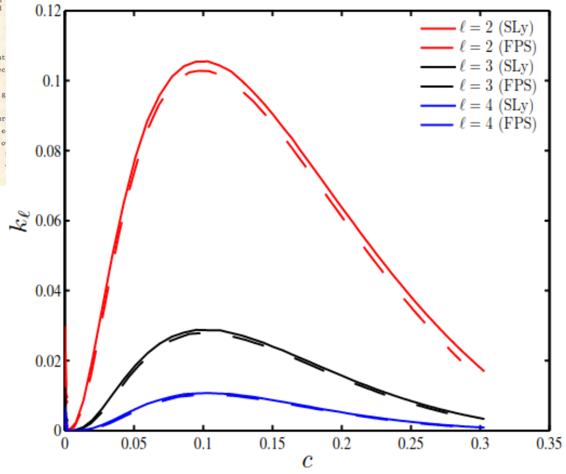

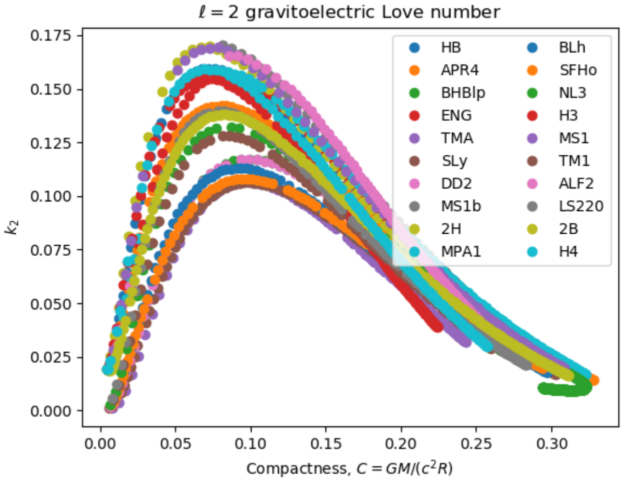

See also Hinderer 2007, Binnington&Poisson 2009

3. DIGEST OF THE HISTORY OF THE PROBLEM OF MOTION

In 1687, I. Newton showed how the orbital motion of approximately spherical extended objects could be well-approximated by the motion of point masses. This is a very important result of Newtonian physics whose extension to General Relativity is highly non-trivial, as was pointed out by M. Brillouin (1922). M. Brillouin called this schematization of an extended body by a point mass with disappearance of all internal structure: "le principe d'effacement" ("effacing principle;" perhaps a more picturesque name would be: "the Cheshire cat principle"). In Newtonian physics the proof of this "effacing principle" makes an essential use of:

1) the linearity of the gravitational field as a function of the matter distribution (which allows one to define and separate the self-field and the external field);
2) the Action and Reaction principle (which allows one to define the center of mass and to ignore the contribution of the self-field to its motion);
3) Newton's theorem on the attraction of spherical bodies.

More specifically, for a binary system constituted of non-rotating nearly spherical bodies of masses m and m', one deduces from 1) that the main correction to the point mass idealization will come from the tidal field $Gm'd^{-3}r$ (where G is Newton's constant, r is the distance away from the center of mass of the first object m, and d is the distance between the two objects). If b denotes the radius of the first object, the tidal field will deform slightly its shape: $\delta b/b = h(m'/d^3)(b^3/m)$, where h, the first Love (1909) number, is a dimensionless quantity of order unity. This deformation induces in turn a small quadrupole moment: $Q = k\, m'b^5d^{-3}$, where k, the second Love number, is a dimensionless quantity of order unity ($h = 3/5$ and $k = 4/15$ for the Earth). Finally this tidally induced quadrupole moment will create a small correction to Newton's law for point masses: $\delta F/F \sim k\,(b/d)^5$. Therefore as long as the radii of the objects are much smaller than their mutual distances, their internal structure (if they are not rotating) will be utterly negligible. We shall show in Section 5 how this result of "effacing" can be extended to Einstein's theory even, and in fact most accurately, in the case of compact objects, i.e. when the radius $b \sim Gm/c^2$. But as we shall not be able to use 1) and 2) above, we shall need a completely different approach to show that the very strong "self field" of the compact object does not contribute to its orbital motion.

Then one can find in vacuum a decoupled second order differential equation for $H = H_0 = H_2$ for instance (Edelstein and Vishveshwara 1970 , Demianski and Grishchuk 1974):

$$\hat{R}(\hat{R}-2)d^2(H/\hat{R}(\hat{R}-2))/d\hat{R}^2 + 3(2\hat{R}-2)d(H/\hat{R}(\hat{R}-2))/d\hat{R} - (L-2)(L+3)\, H/\hat{R}(\hat{R}-2) = 0. \tag{10}$$

The general solution of this second order differential equation contains 2 arbitrary constants. For instance, when $L = 2$, one finds for the general quadrupolar H perturbation in vacuum, i.e. outside the body:

$$H = D(\hat{R}(\hat{R}-2) + k\, \hat{R}(\hat{R}-2) \int_{\hat{R}}^{\infty} 5dx/(x^3(x-2)^3)\ ). \tag{11}$$

The dimensionless constant k is a relativistic generalization (Damour 1981) of the second Love number (Love 1909) which was introduced in Section 3. It is, in a sense, a dimensionless measure of the yielding of the object to an external tidal solicitation. It depends on the internal structure of the body (equations of state,...) and can be determined for an ordinary body (not a black hole) by imposing the regularity of the metric perturbation H, K, h_0 at the center of the body and when crossing the surface of the body (see e.g., Thorne and Campolattaro 1967). By our hypothesis 1) we have $\hat{R} \sim 1$ at the radius of the object, therefore as there are no other scales in the problem, k must be of order unity (like the non-relativistic one):

$$k \sim 1 \tag{12}$$

(More generally for non-necessarily compact objects of dimensionless radius $\hat{b}$, one will have $k \sim \hat{b}^5$ which allows one to justify the remark after hypothesis 1)). In the case of a black hole, k is determined by imposing the regularity of metric perturbation on the future horizon: in this case one finds $k = 0$ (in agreement with D'Eath 1975a). Incidently, one should not conclude from this result that there are no tidal responses of a black hole to an external solicitation: such a non-zero response is contained in the first term of the righthand side of (11): $\hat{R}\,(\hat{R} - 2)$ which differs from the usual term (in absence of any object): $\hat{R}^2$.

The choice of quasiuniversal relation matters

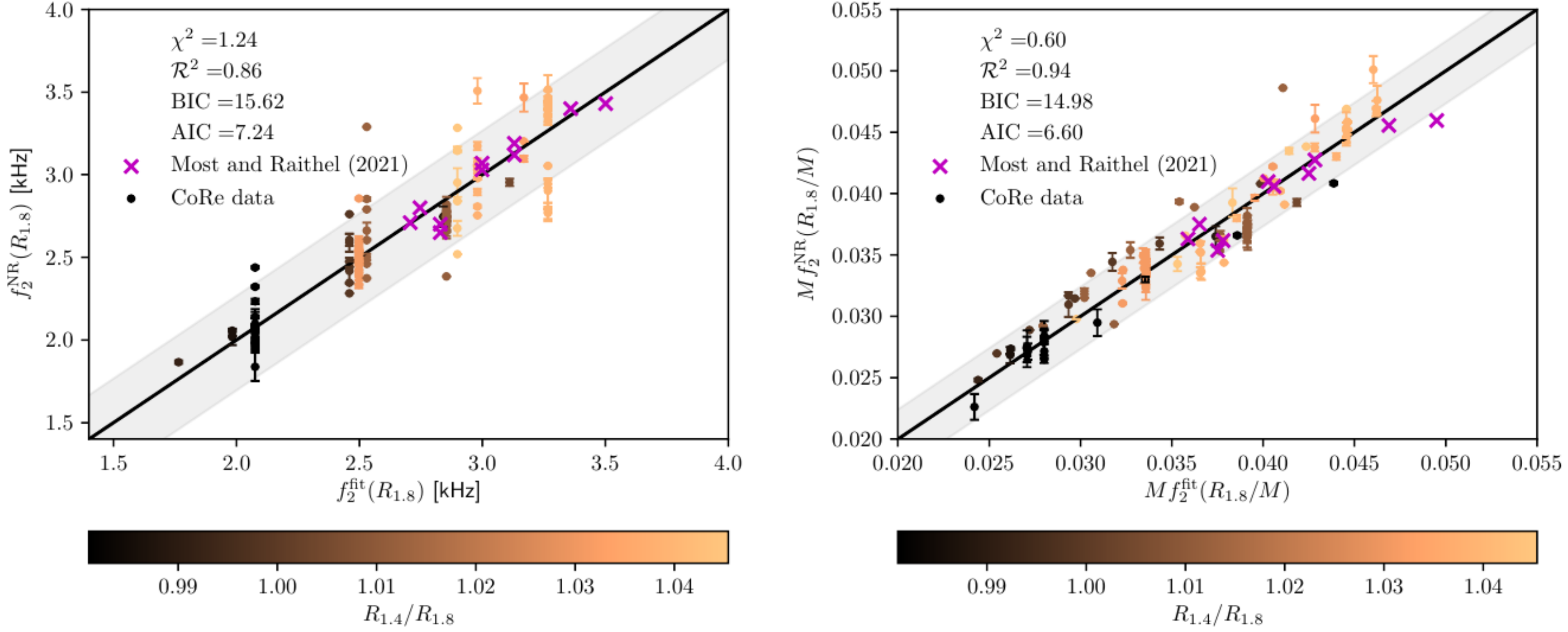

FIG. 8. Predicted values from the calibrated relations Eq. (F1) compared to the respective NR observed quantities. Top panels show $X = 1.4$ and bottom panels show $X = 1.8$. Left panels show non-mass-scaled f_2 and right panels show mass-scaled dimensionless $M f_2$. The diagonal (black line) represents the case in which predictions and observations match and the gray area is the 90% credibility level. The CoRe data are reported with circles colored according to $R_{1.4}/R_{1.8}$ and magenta crosses are the data extracted from [27].